AGU PUBLICATIONS

JGR

Journal of Geophysical Research: Space Physics

RESEARCH ARTICLE

10.1002/2014JA020122

Key Points:
- Ionospheric currents can give only modest contribution to *SYM-H* and *ASY-H* indices
- Region 1 FAC is the main contributor to *ASY-H* index
- *ASY-H* is controlled by interplay between regions 1 and 2 FACs and partial ring current

Supporting Information:
- Text S1
- Figure S1
- Figure S2
- Figure S3
- Figure S4
- Figure S5
- Figure S6
- Figure S7
- Figure S8

Correspondence to:
S. Dubyagin,
stepan.dubyagin@fmi.fi

Citation:
Dubyagin, S., N. Ganushkina, M. Kubyshkina, and M. Liemohn (2014), Contribution from different current systems to *SYM* and *ASY* midlatitude indices, *J. Geophys. Res. Space Physics*, *119*, 7243–7263, doi:10.1002/2014JA020122.

Received 23 APR 2014
Accepted 19 AUG 2014
Accepted article online 22 AUG 2014
Published online 15 SEP 2014

Contribution from different current systems to *SYM* and *ASY* midlatitude indices

S. Dubyagin[1], N. Ganushkina[1,2], M. Kubyshkina[3], and M. Liemohn[2]

[1]Finnish Meteorological Institute, Helsinki, Finland, [2]University of Michigan, Ann Arbor, Michigan, USA, [3]St. Petersburg State University, St. Petersburg, Russia

Abstract Using empirical magnetospheric models, we study the relative contribution from different current systems to the *SYM* and *ASY* midlatitude indices. It was found that the models can reproduce ground-based midlatitude indices with correlation coefficients between the model and real indices being ~0.8–0.9 for *SYM-H* and ~0.6–0.8 and ~0.5–0.7 for *ASY-H* and *ASY-D*, respectively. The good agreement between the indices computed using magnetospheric models and real ones indicates that purely ionospheric current systems, on average, give modest contribution to these indices. The superposed epoch analysis of the indices computed using the models shows that, nominally, the cross-tail current gives the dominant contribution to *SYM-H* index during the main phase. However, it should be remembered that the model region 2, partial ring current, and cross-tail current systems are not spatially demarcated (the systems are overlapped in the vicinity of geostationary orbit). For this reason, this result should be taken with a precaution. The relative contribution from symmetric ring current to *SYM-H* starts to increase a bit prior or just after *SYM-H* minimum and attains its maximum during recovery phase. The *ASY-H* and *ASY-D* indices are controlled by interplay between three current systems which close via the ionosphere. The region 1 FAC gives the largest contribution to *ASY-H* and *ASY-D* indices during the main phase, though, region 2 FAC and partial ring current contributions are also prominent. In addition, we discuss the application of these results to resolving the long-debated inconsistencies of the substorm-controlled geomagnetic storm scenario.

1. Introduction

The indices quantifying the symmetric part of the midlatitude disturbance field, *Dst* [*Suigura*, 1964], and *SYM-H* [*Iyemori*, 1990] are commonly used as a measure of the total storm strength [*Gonzalez et al.*, 1994]. Initial interpretation of the depression of the *Dst* index as an effect of the symmetric ring current (SRC) development was influenced by the Dessler-Parker-Sckopke (DPS) relationship [*Dessler and Parker*, 1959; *Sckopke*, 1966]. It relates the total energy content of the plasma within the inner magnetosphere to a magnetic perturbation at the center of the Earth. However, the role of the SRC in storm time *Dst* dip and applicability of the DPS relation to estimate the value of *Dst* were widely debated during recent decades [*Campbell*, 1996; *Liemohn*, 2003; *Maltsev*, 2004; *Ganushkina et al.*, 2012a] (see also discussion by *Campbell* [2008] and *Liemohn and Chan* [2008]). Some studies suggest that cross-tail current [*Alexeev et al.*, 1996; *Dremukhina et al.*, 1999; *Turner et al.*, 2000; *Alexeev et al.*, 2001; *Ohtani et al.*, 2001; *Maltsev*, 2004; *Ganushkina et al.*, 2004; *Kalegaev et al.*, 2005] or partial ring current [*Liemohn et al.*, 2001; *Liemohn*, 2003] can make prominent or even largest contribution to *Dst* index during main phase. In addition, substorm current wedge also can have a significant effect on *Dst* [*Friedrich et al.*, 1999; *Munsami*, 2000].

The longitudinally asymmetric part of the storm time midlatitude disturbance was extensively studied during the early years of the magnetospheric studies [*Akasofu and Chapman*, 1964; *Crooker and Siscoe*, 1971; *Kawasaki and Akasofu*, 1971; *Fukushima and Kamide*, 1973] and was associated with development of the partial ring current (PRC) in the inner magnetosphere [*Cummings*, 1966; *Cahill*, 1966]. In turn, the PRC development was believed to be a result of energetic particle injection during substorms [*Cahill*, 1966; *Bogott and Mozer*, 1973]. Although, some studies suggested that the asymmetry can be controlled by the balance between region 1 and region 2 currents [*Harel et al.*, 1981; *Crooker and Siscoe*, 1981; *Iyemori*, 1990], many of the scientists nowadays consider the midlatitude asymmetry indices as a measure of the PRC intensity [*Weygand and McPherron*, 2006].

Knowledge of the current systems which contribute to a particular index is important for answering the long-debated question about the storm-substorm relationship. The statistical analysis of substorms during the storm main phase [*Iyemori and Rao*, 1996] showed that the rate of *SYM-H* decrease slowed down just after substorm onset. It was also found that the strength of the symmetric as well as asymmetric *H* component disturbance better correlates with interplanetary magnetic field (IMF) southward component than with auroral electrojet indices *AE* and *AL* [*Russell et al.*, 1974; *Clauer and McPherron*, 1980; *Clauer et al.*, 1983]. At first glance, these findings question the main role of substorms in plasma injection in the ring current region [*Kamide*, 1992]. However, this reasoning is based on the assumption that the symmetric ring current is the only or at least the dominant contributor to the *Dst* index and that the asymmetric disturbance is controlled by the partial ring current resulting from particle injections.

Many studies addressed the question of the sources of the symmetric *H* component disturbance during main phase [*Alexeev et al.*, 1996; *Turner et al.*, 2000; *Liemohn et al.*, 2001; *Tsyganenko and Sitnov*, 2005; *Ganushkina et al.*, 2012b]. Although it is agreed that three current systems (cross-tail current, symmetric, and partial ring currents) are the main contributors but it is unclear which one is the dominant and what fractions of the total index are controlled by the others.

The current systems which produce longitudinal asymmetry at midlatitudes were also discussed. *Fukushima and Kamide* [1973] showed that the main contribution to the *H* component asymmetry comes from field-aligned currents and neither from the ionospheric electrojets nor from the magnetospheric closure current. *Harel et al.* [1981] and *Crooker and Siscoe* [1981] using models and simulation as well as comparison with observations claimed that the net currents at noon and midnight which produce observed asymmetry cannot be considered as simple PRC closure but rather are residual of the regions 1 and 2 current cancellation. *Shi et al.* [2008a, 2008b] showed that strong longitudinal asymmetry which develops during the solar wind dynamic pressure enhancement is produced by the combined effect from regions 1 and 2, PRC, and Chapman-Ferraro currents.

In the present study we use empirical magnetic field models to analyze statistically the relative contribution from the different current systems to the symmetric and asymmetric midlatitude indices. The concise models overview is presented in section 2. For comparison with the models, we use 5 min resolution symmetric (*SYM-H*, *SYM-D*; referred to as *SYM*) and asymmetric (*ASY-H* and *ASY-D*; referred to as *ASY*) indices [*Iyemori*, 1990, 2010]. The procedures of the indices computation from empirical models are described in section 3. Although we start our analysis from the comparison of the model and real indices in section 4, this study should not be considered as a model verification. These models were designed to describe the field of magnetospheric sources in the inner magnetosphere and magnetotail, and the description of the magnetic disturbance on the ground is beyond the model's defined scope. In other words, even if some model is worse in describing the magnetic field on the ground, it still can give a better description in the magnetotail region. In section 5, the local time variations of the model and observed ground midlatitude field are compared. The superposed epoch analysis of the contributions from the different model current systems to symmetric and asymmetric indices is presented in section 6.

2. Brief Comparative Model Overview

2.1. Structure of the Models

We only use empirical models which include the field-aligned currents and dawn-dusk asymmetry. There are three such models hereafter referred to as T01 [*Tsyganenko*, 2002a, 2002b], TS05 [*Tsyganenko and Sitnov*, 2005], and TS07 [*Tsyganenko and Sitnov*, 2007; *Sitnov et al.*, 2008] (we use the storm time version of the TS07 [*Sitnov et al.*, 2008]). All these models were derived fitting the model functions to the large data set of the spaceborne magnetometer vector measurements and concurrent values of the solar wind and IMF parameters and *SYM-H* index. The models aim to describe the average magnetospheric magnetic field as a function of the IMF, the solar wind plasma parameters, and the *SYM-H* index. It should be emphasized here that the description of the magnetic field of the external sources on the ground was by no means a target of the modeling. For this reason, the ionospheric currents were not considered and the spacecraft database does not include the data closer than $r \approx 3$–$4\ R_E$.

At the first glance, the comparison of the model-based and real *SYM-H* indices looks unjustified since the models themselves are parameterized by the *SYM-H* index. However, it should be noted that (1) the models represent the field of magnetospheric current systems, while the real *SYM-H* index can be affected also

by ionospheric current systems and the currents induced in the ground. (2) The *SYM-H* index is not the only parameter of the model; moreover, in the TS05 model the dependence on *SYM-H* is minimized (*SYM-H* is used only for parameterization of the geometrical properties of the current systems while their intensities depend solely on IMF and solar wind). (3) The fact that some of the model systems are parameterized by *SYM-H* indicates that this current system varies in accordance with *SYM-H*. It is possible that it gives a negligible contribution to the variation of the ground magnetic field or it gives only some fraction of the variation.

A few factors are critical for the magnetospheric model quality. Among them, the main factors are (1) the ability of the model functions to resolve the spatial variations, (2) to describe the response of the magnetosphere to the change of external conditions (solar wind and IMF parameters), and (3) the size and quality of the data set the model was fitted to. Every model addresses these problems in a specific way. The T01 and TS05 models comprise a few modules; each module represents one of the conventional current systems (see *Tsyganenko* [2002a] for the modules description). Throughout the paper, the following abbreviations are used for the model modules: DS (Dipole Shielding), a magnetopause current system shielding the field of the Earth's dipole inside the magnetosphere; TAIL, a cross-tail current; R1 and R2, region 1 and region 2 field-aligned currents; SRC, a symmetric ring current; and PRC, a partial ring current.

The module functions have nonlinear parameters controlling the geometry of a corresponding current system (equatorward shift of the regions 1 and 2 FAC zones, cross-tail current thickness, and the earthward shift of its inner edge, etc). The field of every module includes the contribution of the shielding magnetopause currents, so that the resulting module field has zero normal component on the magnetopause. This feature allows one to compute the total model field as a linear sum of the fields of different modules with arbitrary linear coefficients; the resulting configuration stays shielded inside the magnetopause. The linear coefficients determine the intensity of the corresponding current systems.

In contrast, the magnetic field of the equatorial currents in the TS07 model is expanded into a sum of the basis functions of different scales which have no physical meaning. However, the advantage of this approach is that the sum of these basic functions can describe arbitrary azimuthal and radial magnetic field variation. The equatorial current field is also naturally complemented by the regions 1 and 2 FACs whose azimuthal dependence is represented as sine and cosine harmonics of the magnetic local time (MLT). Each of these systems is also shielded inside the magnetopause, and the resulting model field is a sum of the functions with linear coefficients. The basis functions and regions 1 and 2 FAC elementary harmonics also have nonlinear parameters defining their geometrical characteristics.

2.2. Models Parameterization

In section 2.1 we described the general structure of the models. A set of parameters defines the relative intensity of the current systems and their geometry. In addition, the models have to respond somehow to a change of external conditions or/and to the levels of geomagnetic activity (magnetospheric indices). Generally, it is assumed that the state of the magnetosphere, to some extent, can be defined by some combination of the solar wind velocity, density, IMF, and *SYM-H* index. Different approaches are used to introduce these dependencies in the models.

In the TS07 model, the main data set of spacecraft measurements is binned according to the modeled conditions. The model is parameterized by ~6 h weighted averages of the solar wind electric field $\langle VB_S \rangle$, $\langle SYM\text{-}H \rangle$, and its derivative $\langle \mathrm{d}SYM - H/\mathrm{d}t \rangle$ [*Sitnov et al.*, 2008] (the model also accepts P_{dyn}, but it is not used for data binning). For every modeled moment, the subset of the main database of the spacecraft observations is selected with corresponding parameters close to those for the modeled time (so called "nearest neighbor approach"). After that, the set of the model coefficients is found by minimizing the difference between the model and the subset of the data (see also http://geomag_field.jhuapl.edu/model/). Thus, the model coefficients have to be determined for every modeled time. By now, the model coefficients are available for the set of eight storms. This approach places great requirements to the size of the main data set, since every combination of the model parameters for the modeled event has to be well represented in the main database by its nearest neighbors. This is because the subset of the nearest neighbors should have a good coverage of the magnetosphere to resolve the characteristic features of the magnetic field spatial variations for the modeled moment. The size of the main data set limits the model spatial and temporal resolution. Although the input parameters are computed as averages over a characteristic time scale of $\geq$ 6 h [*Sitnov et al.*, 2010], time resolution of the model is 1 h.

Table 1. Model Characteristics

	T01	TS05	TS07
Spacecraft Data the Models Were Fitted to			
Specific Events	All Data	Storms Only	Binned[a]
# of Data Points	45,202	142,787	1,145,754
Epoch	1984–1999	1996–2000	1994–2005
Representation of the FACs in the Models			
R1	$\sin(m\varphi)$ $m = 1, 2$	$\sin(m\varphi)$ $m = 1$	$\sin(m\varphi)$ $m = 1, 2$
R2	$\sin(m\varphi)$ $m = 1, 2$	$\sin(m\varphi)$ $m = 1$	$\sin(m\varphi)$ $\cos(m\varphi)$ $m = 1$
PRC	Yes	Yes	No

[a]Binned according to modeled conditions. See explanations in the text.

T01 and TS05 consist of the same set of the current systems and use essentially the same functions for their mathematical description. In contrast to TS07 model, the solar wind parameters are treated as continuous variables in these models. That is, the model coefficients, in turn, are represented as functions of the solar wind and IMF parameters and *SYM-H* with free coefficients. Although the number of the model free parameters increases, the model can be fitted to the whole data set of the spacecraft measurements and concurrent solar wind and IMF parameters and *SYM-H*. The T01 model uses as input the 5 min averages of the solar wind dynamic pressure, *SYM-H* index, *Y* and *Z* components of the interplanetary magnetic field and two parameters (G_1, G_2) characterizing the conditions in the solar wind during an hour preceding to the modeled time. The G_2 parameter is a 1 h average of $V \cdot |B_S|$, where B_S is the southward component of the IMF and V is solar wind velocity. $G_2 \approx \langle VB_\perp^2 \sin^3(\Theta/2)\rangle$ (see *Tsyganenko* [2002b] for details).

The most advanced method of the model parameterization with the solar wind drivers is developed in the TS05 model. Although the general approach is the same as in T01 (model geometry/intensity coefficients are functions of the solar wind parameters), there are much fewer preassumptions about the functional form of the solar wind driving parameters. It is assumed that the response of current systems is proportional to some power of solar wind density, velocity, and southward IMF component ($N^\alpha V^\beta B_S^\gamma$). In addition, it is assumed that every current system has a certain exponential decay rate (r), so the model input parameter for a particular system (W) is computed as a time integral with exponential weight function $W(t) = \int_0^t N(\tau)^\alpha V(\tau)^\beta B_S(\tau)^\gamma \exp(r(t-\tau))\mathrm{d}\tau$. The integration starts from the last geomagnetically quiet interval. Finally, to take into account the saturation, the input parameter enters the model in the form $W/\sqrt{1+(W/W_C)^2}$, where W_C is the threshold for saturation. For every current system, the α, β, γ, r, and W_C coefficients are treated as unknown variables which are found after fitting to the experimental data.

The top part of Table 1 specifies the data set of the spacecraft data the models were fitted to. The T01 model was fitted to all data available, while the TS05 was fitted only to the data taken during 37 major storms. The second line is the total number of data records, and the third line is the time interval. It can be seen how the amount of available data grows with time. Although the TS07 data set is largest, it should be remembered that, for every moment, the model was fitted to a smaller subset. The size of this subset was ~8000 records [*Sitnov et al.*, 2008] that is even smaller than the T01 data set.

The models are the most accurate in the regions of physical and parameter space where the most real measurements are available for the fitting procedure. Since the T01 database includes all observations, the model is the most accurate for typical parameters of the solar wind and less accurate for the extremal conditions. The TS05 model database includes only the periods of geomagnetic storms with a couple of days preceding the events. For this reason, its accuracy is not so strongly dependant on the magnetospheric activity level.

It should be noted that the bad agreement with the magnetic field measurements in the magnetosphere does not automatically mean that the agreement with the ground-based magnetic field measurements and indices will be also bad. The opposite is also true. For example, during a storm interval, the models often show a prominent disagreement with spacecraft observations in the vicinity of the equatorial plane which can be as large as ~50 nT [*Huang et al.*, 2008]. It basically happens because the cross-tail current sheet is very thin and dynamic during active periods. Its vertical location and thickness is very difficult to predict. On the other hand, there is a strong magnetic field gradient in the vicinity of the current sheet and even a

Table 2. List of Ground-Based Observatories and Normalization Coefficients for *ASY* Indices Computation[a]

Observatory	Geo.Lat	Geo.Lon	Geomag.Lat.	Geomag.Lon.	$C_i^{(H)}$	$C_i^{(D)}$
SanJuan (SJG)[b]	18.1	293.9	28.4	5.9	1.01	0.97
Fredericksburg (FRD)	38.2	282.6	48.4	353.1	1.11	1.00
Tuscon (TUC)[b]	32.2	249.3	39.8	315.8	0.92	0.97
Boulder (BOU)	40.1	254.8	48.3	320.3	1.26	1.02
Honolulu (HON)[b]	21.3	202.0	21.5	269.5	0.99	1.20
Memambetsy (MMB)[b]	43.9	144.2	35.0	211.0	1.00	1.00
Alibag (ABG)[b]	18.6	72.9	9.9	146.0	0.99	1.20
Hermanus (HER)[b]	−34.4	19.2	−33.7	83.7	0.97	−0.89

[a]The geomagnetic coordinates are computed for the epoch 2000.
[b]Observatories used for computation of the model indices.

small difference between the model and real current sheet positions leads to a significant disagreement in the magnetic field. However, this effect decreases fast with distance from the regions of the strong magnetic field gradients. The magnetic field on the Earth's surface, therefore, is not sensitive to the variations of the vertical position and thickness of the cross-tail current sheet.

2.3. Field-Aligned Currents

The field-aligned currents are believed to give significant contribution to the local time asymmetry of the ground midlatitude *D* and *H* components. All three models have the large-scale FAC modules. The local time dependence of the R1 and R2 currents in T01 and TS05 models is purely antisymmetric relative to noon-midnight meridian plane. The bottom part of Table 1 shows the order and type of the harmonics used for modeling R1 and R2 systems. However, during the main phase of the geomagnetic storms, the partial ring current shifts into the dusk sector, and its distribution cannot be described by a sine function. For this reason, the separate PRC module is introduced in the T01 and TS05 models. Although the physical mechanism of the PRC and R2 currents are essentially the same, the PRC module field-aligned closure currents are put a bit more equatorward relative to the R2 zone. This artificial discrimination has been eliminated in the TS07 model, where the storm time PRC effect is described by adding a cosine harmonic to the R2 current. The bottom line of Table 1 indicates a presence of a separate PRC module in the models. The table shows that the T01 model has the highest azimuthal resolution (employs second-order harmonics) of the large-scale FAC modules.

The separate azimuthal harmonics are treated as separate current subsystems. In the T01 model, the linear coefficients defining the current intensity for particular subsystem are linear functions of the G_2 parameter. In the TS05 model, these coefficients are functions of the specific *W* parameter, computed for a particular system as described in section 2.2. Apart from the FACs intensity, the magnetic effect of the regions 1 and 2 current system at midlatitudes depends also on the width of the their ionospheric projection. In the T01 model, the nonlinear parameters controlling the equatorward shift of the regions 1 and 2 zones are also functions of the G_2 parameter. In the TS05 model, these parameters are proportional to the pressure-corrected *SYM-H* index. In the TS07 models, all linear coefficients as well as nonlinear parameters are found for every modeled moment after fitting to the corresponding "nearest neighbor" subset.

It should be noted that the description of the magnetic disturbance on the ground was not a priority when these models were created. For simplicity, all FAC systems close via the Earth's center. Moreover, the models do not include explicitly the substorm current wedge system. However, the averaged effect of the substorm current wedge might be implicitly present in the models.

3. Calculations of Model *SYM* and *ASY* Indices

When calculating the model *SYM-H* and *ASY-H* indices, we tried to make our procedure as close as possible to that used for real indices at the World Data Center for Geomagnetism, Kyoto (http://wdc.kugi.kyoto-u.ac.jp/aeasy/asy.pdf, hereafter *Iyemori* [2010] [see also *Iyemori*, 1990]). We obtain the model magnetic field at the locations of six geomagnetic observatories listed in Table 2. The derivation procedure for real indices consists of the four steps, and we reproduce every step with the models as follows:

1. Subtraction of the quiet day variation which includes main geomagnetic field, the solar quiet day variation (*Sq*), and quiet day variation of the external sources field. The models used in this study provide the external magnetic field at the locations of the stations, and there is no need to subtract the main field as well as *Sq* variation. However, it is necessary to subtract the quiet day variation of the external field. To determine this variation for every observatory, we use the T01 model with input parameters corresponding to a quiet period. This model was chosen because quiet time periods are well represented in the data the model had been fitted to [*Tsyganenko*, 2014]. However, our tests showed that using the TS05 model for the quiet time baseline determination does not change the results presented in the following sections except for a bit lower correlation coefficients found in section 4. According to the *Iyemori* [2010] procedure, to calculate the quiet day variation, the data of five international quiet days are used. We use a bit different approach defining the model input parameters for quiet time once and for all. First, the *SYM-H*, IMF, and solar wind parameters were selected for five quietest days of every month with storms presented in the *Turner et al.* [2009] list. Then, these parameters were averaged over the whole subset and used as quiet time model parameters. The list of five quietest days for every month can be found at http://www-app3.gfz-potsdam.de/kp_index/qddescription.html. Since T01 accepts the instant values of *Pd*, *SYM-H*, B_Y, and B_Z IMF and 1 h mean for computation of the G_1 and G_2 parameters, we use the median average for *Pd*, *SYM-H*, B_Y, and B_Z IMF and mean average for the *G* parameters. The determined quiet time T01 parameters were $Pd = 1.45$ nPa, $Dst = -2$ nT, $B_Z = 0.75$ nT, $G_1 = 1.02$, and $G_2 = 1.02$. We set $B_Y = 0$ to zero. Finally, for every moment of time (t_k), we computed the disturbance of the model field at the *i*th observatory position as $d\mathbf{B}_i = \mathbf{B}_i(t_k)^{\mathrm{DIST}} - \mathbf{B}_i(t_k)^{\mathrm{QUIET}}$. Here the models with the input parameters determined for the time t_k and the model with quiet time parameters specified above are designated by indices "DIST" and "QUIET," respectively.
2. Coordinate transformation to a dipole coordinate system. Our models are able to provide the model magnetic field components in dipole (geomagnetic) coordinates, so no specific rotation is necessary. We define dH_i and dD_i as the dipole northward and eastern components of the vector $d\mathbf{B}_i$.
3. Calculation of the longitudinally symmetric component. The longitudinally symmetric component is calculated by averaging the disturbance component for six stations. For *SYM-H*, a latitudinal correction is made (λ_i is the dipole latitude of each station):

$$SYM\text{-}H = \frac{\sum_{i=1}^{6} dH_i}{\sum_{i=1}^{6} \cos(\lambda_i)} \tag{1}$$

$$SYM\text{-}D = \left(\sum_{i=1}^{6} dD_i\right)/6 \tag{2}$$

4. Calculation of the asymmetric component. The asymmetric variation at each station is obtained by subtracting the symmetric component from the disturbance field. In case of the *H* component, the latitudinal correction is done before subtraction. In addition, for every station normalization coefficients are introduced for both *H* and *D* components as shown below:

$$\delta H_i = \left(\frac{dH_i}{\cos(\lambda_i)} - SYM\text{-}H\right) \cdot C_i^{(H)} \tag{3}$$

$$\delta D_i = \left(dD_i - SYM\text{-}D\right) \cdot C_i^{(D)} \tag{4}$$

here $C_i^{(H)}$ and $C_i^{(D)}$ are the normalization coefficients for a particular station. For the real *ASY* index derivation, *Iyemori* [2010] determined these coefficients empirically as the standard deviation at the stations became equal. We used the coefficient provided by T. Iyemori (private communication, 2012) and listed in Table 2. For the station in the Southern Hemisphere the sign of the δD_i is reversed (the $C_i^{(D)}$ coefficient is negative for Hermanus station). However, these coefficients are probably affected (among the other things) by the Earth's conductivity at a given station, which is not included in the model. Finally, the

ASY-H index is calculated as the difference between the maximum and minimum asymmetric variations among all stations:

$$ASY\text{-}H = \max_i(\delta H_i) - \min_i(\delta H_i) \quad (5)$$

$$ASY\text{-}D = \max_i(\delta D_i) - \min_i(\delta D_i) \quad (6)$$

The T01 and TS05 models consist of separate modules representing the fields of conventional current systems (see section 2.1 for details). This feature allows to study the relative contribution of the model current systems to the geomagnetic indices. Our computations of the contribution from a particular system is generally equivalent to that for the total model index. More specifically, when we compute the disturbance field (step 1), we only use the field of a particular model module for both disturbed and quiet time values. After that, we repeat steps 1–4 as described above. Since both models comprise equivalent sets of the current systems, we always use the T01 model for determination of the quiet time baseline of a module field.

It should be noted that for *ASY* indices this method gives the maximum midlatitude magnetic field asymmetry which a particular current system can give. Although the asymmetries of all systems are positive by definition, they can compensate each other if the systems have the asymmetries of opposite sense (for example, R1 and R2 FAC systems). In other words, while for the *SYM* indices a total model index is a sum of contributions from the separate modules, this is not true for *ASY* indices.

However, when comparing the real indices with those computed from the models, it is necessary to take into account the contribution of the electric currents induced in the ground. The variable field of the magnetospheric and ionospheric sources induces the currents inside the Earth in the conducting rocks at a few hundreds kilometers depth. The magnetic field of these currents in turn amplifies the horizontal component of the magnetic field on the surface. As a result the magnetic field variations measured on the ground include both the field of the external sources and the field of induced currents. This additional contribution depends on the field variation time scale as well as on the details of the conductivity distribution under a particular observatory. *Häkkinen et al.* [2002] estimated that the contribution of the ground-induced currents to 1 h resolution *Dst* index is ~25–30%. Having no other information about this contribution, we use this estimate in our study. In addition, we also present a result of the independent tentative test of the reliability of this estimate in section 4.2.2.

4. The Comparison of the Model and Real Indices

4.1. Case Study: 31 October 2005

Before starting to use the empirical models for estimation of the contributions from the current systems to the indices, we need to check how well the models reproduce the real indices. We start our analysis with the case study of the moderate storm on 31 October to 2 November 2005. Figures 1a and 1b show the evolution of the IMF components and solar wind dynamic pressure. The solar wind velocity (not shown) was ~400 km/s. The black, thick curves in Figures 1c–1f show real *SYM* and *ASY* indices. The *SYM-H* index attains a value of −76 nT (Figure 1c), and this moment is marked by a vertical dashed line. The main phase of the storm followed after IMF B_Z turned southward at ~0800 UT on 31 October 2005 (the B_Z reached −9 nT at ~1615 UT).

The parameters of the T01 and TS05 models as well as a table of the precomputed coefficients for the TS07 model were available for this storm. Using the algorithm described in section 3, the *SYM* and *ASY* indices were computed for all three models. The model indices were divided by 0.8 to take into account 25% contribution of the ground induced currents (see section 3). The green, red, and blue curves in Figures 1c–1f correspond to the T01, TS05, and TS07 model indices, respectively. It can be seen that all models reproduce the *SYM-H* index minimum value very well. It should be remembered that the estimation of the contribution from geomagnetically induced currents in the ground is very coarse. The T01 model is the best for reproducing the time variation of the *SYM-H* index while TS05 and TS07 sometimes overestimate the strength of *SYM-H* disturbance. Figure 1d shows the model and real *ASY-H* index comparison. Although all models show variations similar to the real *ASY-H* index, the general agreement is worse than that for the *SYM-H* index. The *SYM-D* index is rarely used because its amplitude is generally much weaker than that for *SYM-H*. It is surprising that the models generally reproduce the variation of *SYM-D* index for this event (Figure 1e)

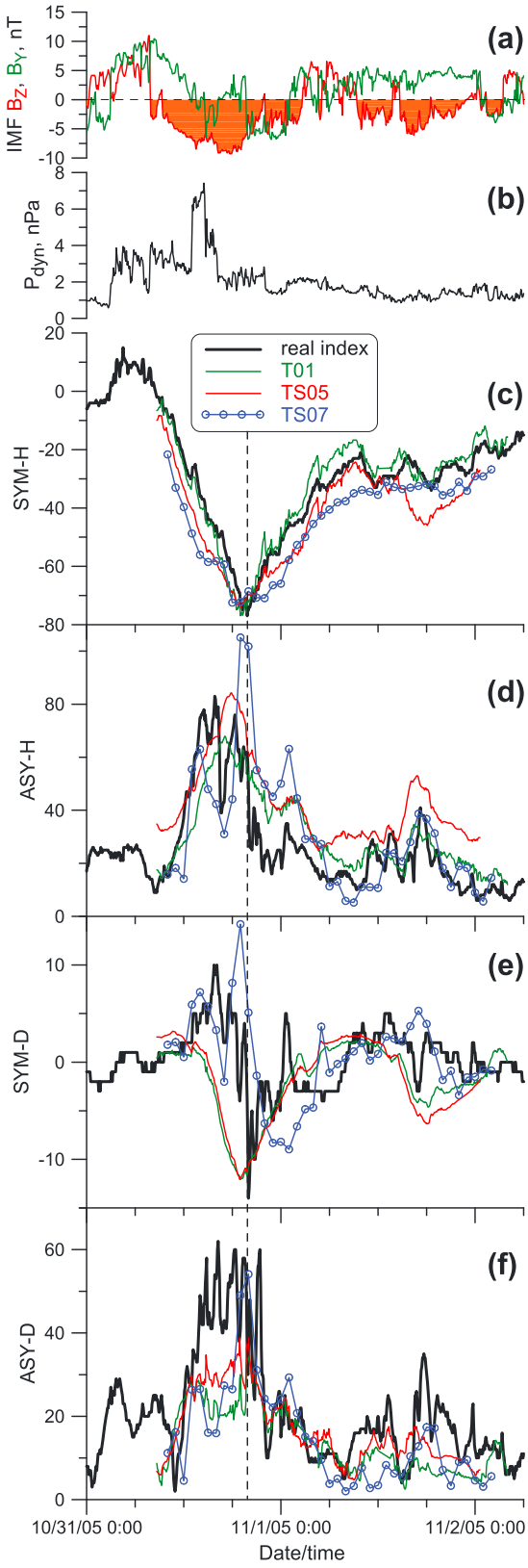

Figure 1. (a) IMF B_Z (red) and B_Y (green) GSM components. (b) Solar wind dynamic pressure. (c–f) The comparison of the real indices (black curves) and those computed using three empirical models (T01 (green), TS05 (red), and TS07 (blue)).

albeit the timing is not accurate. Figure 1f shows model and real *ASY-D* indices. All models failed to reproduce the index peak values except for TS07 which did it only for short period. However, the models were close to the real index during early main phase and the recovery phase.

4.2. Statistical Study

4.2.1. Events Selection

Although the results presented in section 4.1 show that the models generally reproduce the variations of the real indices, a quantitative statistical study is needed. We use two subsets of the storm events. First, we use the list of eight storms during 2001–2011 with the TS07 coefficients available from http://geomag_field.jhuapl.edu/model/storm_list.html to compare three models (hereafter referred as Sitnov's list). Second, we use the list of the corotating interaction region (CIR)- and coronal mass ejection (CME)-driven storms with min(*Dst*) < −50 nT [*Turner et al.*, 2009] (hereafter referred as Turner's list). It covers the periods 1995–2004 and includes ~200 storms (among them a few superstorms with *SYM-H* < −300 nT). However, *Turner et al.* [2009] used *Dst*, while we use the *SYM-H* index. *Katus and Liemohn* [2013], however, found that these two disturbance measures have a random difference of ~10 nT, increasing to ~20% during storm intervals. Therefore, for some storms from the Turner's list min(*SYM-H*) > −50 nT and the data for those storms were discarded. The time spans given in the list include the period from sudden commencement until the end of recovery. However, in our study we focus only on the main and recovery phases. The main and recovery phase periods for every storm were defined in the following way: The time of *SYM-H* minimum was determined. Then, we traced *SYM-H* backward and forward in time until it exceeded −10 nT threshold, defining the periods between the *SYM-H* minimum and these times as main and recovery phases.

Turner's list discriminates CME- and CIR-driven storms, and it would be interesting to compare the model index response to these two different types of storms. It is known that CME storms tend to produce a stronger *Dst* dip [*Borovsky and Denton*, 2006] and direct comparison of the data sets

Table 3. Comparison of the Model and Real Indices

	SYM-H	*SYM-D*	*ASY-H*	*ASY-D*
	Correlation Coefficients for Sitnov's List			
T01	0.94	0.32	0.81	0.56
TS05	0.89	0.41	0.78	0.64
TS07	0.83	0.16	0.62	0.45
	Correlation Coefficients for Turner's List			
T01	0.91	0.09	0.66	0.44
TS05	0.89	0.49	0.74	0.64
	Correlation Coefficients for Peak Values			
T01	0.94		0.67	0.65
TS05	0.94		0.79	0.68
	Ratio of Model to Real Indices			
T01	1.07–1.14		1.07–1.72	2.00–5.24
TS05	0.74–0.77		1.03–1.20	0.60–0.74
T01[a]	0.95–0.98		0.77–0.87	0.75–1.15
TS05[a]	0.82–0.84		0.91–1.01	0.55–0.62

[a]The values for subset of the storms with min *SYM-H* > -200 nT.

would rather reflect the difference between stronger and weaker storms. To eliminate this bias, we created normalized subsets of the Turner's list. We started from plotting the histograms of the CME and CIR storms strength (as measured by min *SYM-H*) with 10 nT bin size. For every bin, we randomly removed certain number of the CIR or CME storms so that their numbers after removal were equal. After this procedure, we have subsets of the CIR and CME storms with similar distributions of the storm strengths. Hereinafter, when we discuss the comparison of the CIR and CME storms, we will implicitly refer to these normalized data sets.

4.2.2. The Results of Statistical Comparison

We start from the comparison of the models for the list of eight storms in 2001–2011 (Sitnov's list). Using the algorithm described in section 3, the *SYM* and *ASY* indices were computed for all three models. Generally, for every storm from the list, the TS07 coefficients are available also for some period before and after the storm. We selected the main and recovery phases as it is described in section 4.2.1. Since the TS07 model has a 1 h time resolution, the indices computed for the T01 and TS05 models as well as the real indices were averaged over 1 h for synchronization with the TS07 model indices. If the indices could be computed only for one or two models, we discard these data to make the data sets for all three models fully synchronized.

The top part of Table 3 shows correlation coefficients between the real indices and the indices computed using the models. For all three models, the best correlation is achieved for the *SYM-H* index (0.83–0.94) and the worst correlation is for the *SYM-D* index (0.16–0.32). All the models show better correlation for *ASY-H* (0.62–0.81) than *ASY-D* (0.45–0.64). The T01 model shows better correlation for *H* component indices, while the TS05 model shows better performance for the *D* component. However, Sitnov's list covers only eight storms of similar strength with min *SYM-H* ≈ -100 nT, and it would be interesting to check the model performance for a wider range of conditions. The second part from the top of Table 3 shows correlation coefficients for Turner's list of storms computed for the T01 and TS05 models with 5 min resolution. It can be seen that the T01 model shows better correlation only for *SYM-H* index while the TS05 is better for *SYM-D*, *ASY-H*, and *ASY-D*.

However, a good correlation just indicates that two values vary in a similar way. To check whether the model and real indices quantitatively agree, we compare their extremal values during every storm. For every storm and for every index, we determined the peak values of the model and real indices (minimum for *SYM-H* and maximum for *ASY-H* and *ASY-D*. It should be noted that the real and model indices often attain their peak values at different times (See Figure 1). This difference can be as large as a few hours for the *ASY* indices.

Figure 2 shows the peak values of model indices versus those for real indices in a double logarithm scale. Figures 2a and 2b, Figures 2c and 2d, and Figures 2e and 2f correspond to *SYM-H* (we use absolute value), *ASY-H*, and *ASY-D* indices, respectively. Figures 2a, 2c, and 2e and Figures 2b, 2d, and 2f correspond to the T01 and TS05 model indices. The correlation coefficients are shown in Table 3 (the third part from the top). It can be seen that correlation coefficients for peak values are a bit higher than those for a whole index variation (for Turner's list, Table 3). To check the quantitative agreement of the model and real indices, we fitted the data points in Figure 2 using the linear functions $Y_i = A \cdot X_i$, where Y_i and X_i are model and real index peak values, and A is a free parameter. According to *Häkkinen et al.* [2002], the contribution of the induced currents in the Earth is ~25%. Hence, we expect $A \approx 0.8$. We tried ordinary least squares fitting with ΔY and ΔX minimization. The two top lines of the bottom part of Table 3 show the obtained values of A. It can be

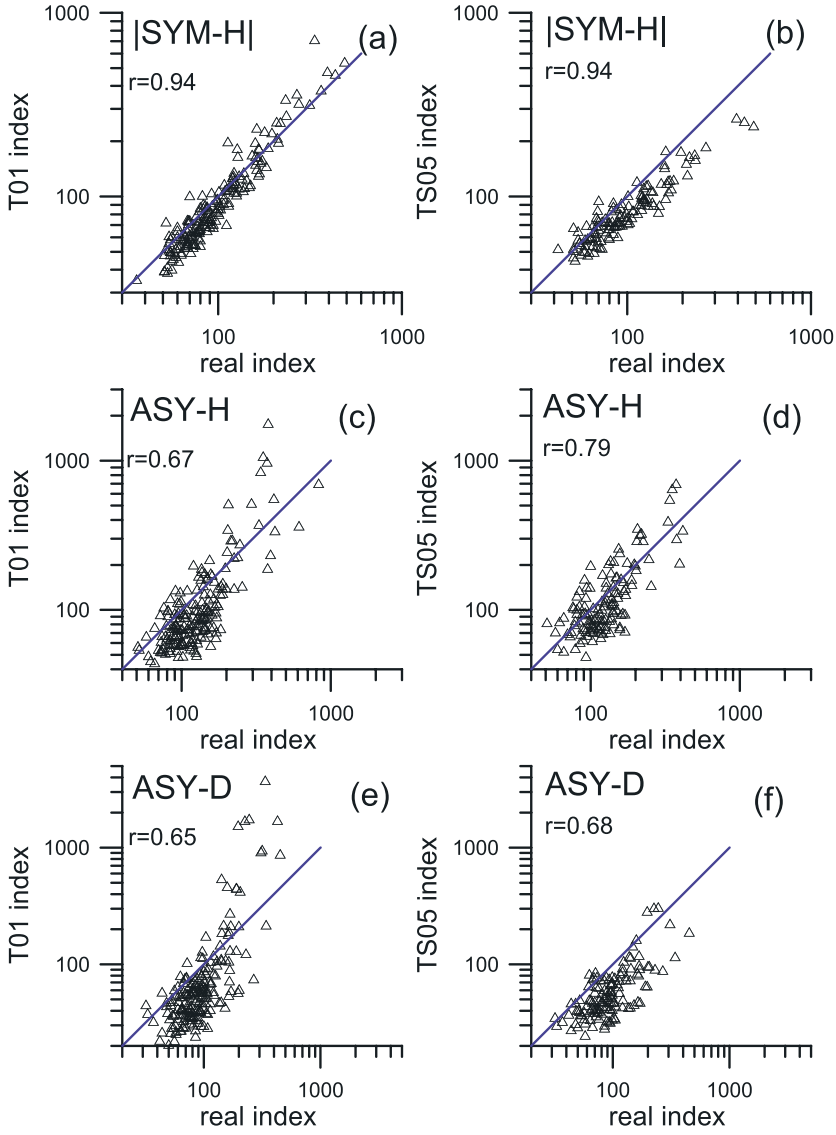

Figure 2. The peak values of the indices, model versus real, for Turner's list of storms. Blue lines show one to one dependence.

seen that the T01 model tends to overestimate the indices, while the TS05 slightly overestimates the *ASY-H* index. The deviation from linear dependence can be seen in Figure 2 for the strongest storms. We also computed the *A* values for a subset of the storms with min *SYM-H* > -200 nT. The resulting values are presented in the two bottom lines of Table 3. It can be seen that the models show much better agreement with real indices for moderate storms. The TS05 gives an almost perfect (0.82–0.84) ratio of the model to real indices for *SYM-H* while T01 shows plausible values (0.77–0.87) for *ASY-H*.

Although it is difficult to carry out strict analysis of the model index accuracy since the effect of the induced currents is never accurately known, we performed tentative estimation using 0.8 coefficient for the TS05 model indices. The relative model error was computed using the following equation:

$$\text{rel.err} = \left| \frac{\text{real index} - \text{model index}/0.8}{\text{real index}} \right| \cdot 100\% \tag{7}$$

The rel.err values were computed for Turner's list for all data satisfying criterion |real index| > 45 nT. Median values of rel.err were 0.17%, 0.31%, and 0.39% for *SYM-H*, *ASY-H*, and *ASY-D*, respectively. We also computed

an absolute error as

$$\text{abs.err} = \left(\frac{1}{N} \sum_i \left(\text{real index}_i - \text{model index}_i / 0.8 \right)^2 \right)^{\frac{1}{2}} \quad (8)$$

No limitation on the index value was applied. We found 21 nT, 44 nT, and 22 nT values of abs.err for *SYM-H*, *ASY-H*, and *ASY-D*, respectively.

In addition, the correlation coefficients and the errors were compared separately for the CME and CIR storms lists. However, we found only minor differences between these two subsets.

5. The Comparison of Local Time Variations of the Ground Midlatitude Field and Model Predictions

The *ASY* indices provide information only on the amplitude of the local time asymmetry (difference between maximum and minimum values) but not on its orientation (local time of the maximum or minimum). For this reason, the rather high-correlation coefficients found in section 4 do not mean that the model reproduces the ground midlatitude magnetic field well. For this reason, we compare the model field with the observation at the particular observatories. We selected 10 moderate storms from Turner's list. The data from the eight midlatitude observatories (listed in Table 2, the same observatories which are used for computation of the real *SYM* and *ASY* indices) were acquired from the INTERMAGNET network. We used the so-called *definitive data* (see documentation at www.intermagnet.org). Depending on an observatory and a year, the original data were presented in the geographic or magnetic coordinate system and were converted into spherical geomagnetic coordinates. The quiet time variations were determined for every observatory using the list of the five quietest days of a month (http://www-app3.gfz-potsdam.de/kp_index/qddescription.html). Using the data during these five days, we computed the median value of the *H* and *D* components during every hour. Then, we computed the quiet time daily variation at 5 min resolution using linear interpolation between these points. This quiet time variation was subtracted from the measurements during storm time. The resulting disturbance field components are denoted by *dH* and *dD*. After that, the *dH* component for every observatory was divided by the cosine of the observatory geomagnetic latitude. A disturbance in the *D* component from an ideal symmetric FAC system has opposite signs in different hemispheres and vanishes at the equator. For this reason, we inverse the sign of the *dD* for the stations in the Southern Hemisphere.

To determine the asymmetry orientation, or in other words asymmetry phase angle, we use the observation at six stations distributed almost evenly in local time (marked by *a* symbol in Table 2). If the data for San Juan or Tucson were not available, we used the data from Fredericksburg and Boulder observatories, respectively. The San Juan and Fredericksburg observatories (as well as Tucson and Boulder) are located at close magnetic longitudes, and the coverage of local time sectors remains more or less even. The values of *dH* and *dD* at these six stations were fitted using the equation $A \cdot \sin(\varphi + \delta) + B$ for every moment of time. Here *A*, *B*, and δ are free parameters and φ is the MLT of the observatory expressed in angular units. Since $\sin(\varphi) = -\sin(\varphi + \pi)$, we allowed only positive values for *A* to avoid ambiguous solutions. For *dD*, the value of the parameter $\delta = 0$ (asymmetry phase angle) corresponds to the asymmetry expected for the FAC region 2 type system which produces eastward magnetic field on the dawnside and westward field on the duskside. On the contrary, $\delta = \pi$ corresponds to the FAC region 1 sense asymmetry.

The fitting procedure was carried out for both model field and real observations. Figures 3a and 3b show the histograms of *dH* asymmetry phase angle of the model and real observations. Black histograms correspond to the observations, and red corresponds to model field asymmetry. Figures 3a and 3b show a comparison of the observations with the T01 and TS05 models, respectively. Figures 3c and 3d show asymmetry phase angle for *dD* local time variation in the same format as in Figures 3a and 3b. The model and observation data sets presented in every histogram are fully synchronous. However, the number of points when model parameters are available is generally higher for the T01 model in comparison to TS05. For this reason, the number of events in every bin is higher in Figures 3a and 3c.

The phase angle of the asymmetry of the observed field agrees well with the results of *Iyemori* [1990]. Roughly, *dH* variation on average is asymmetric with respect to noon-midnight meridian while *dD* is asymmetric with respect to dusk-dawn meridian. The distribution for the T01 model is centered very close to

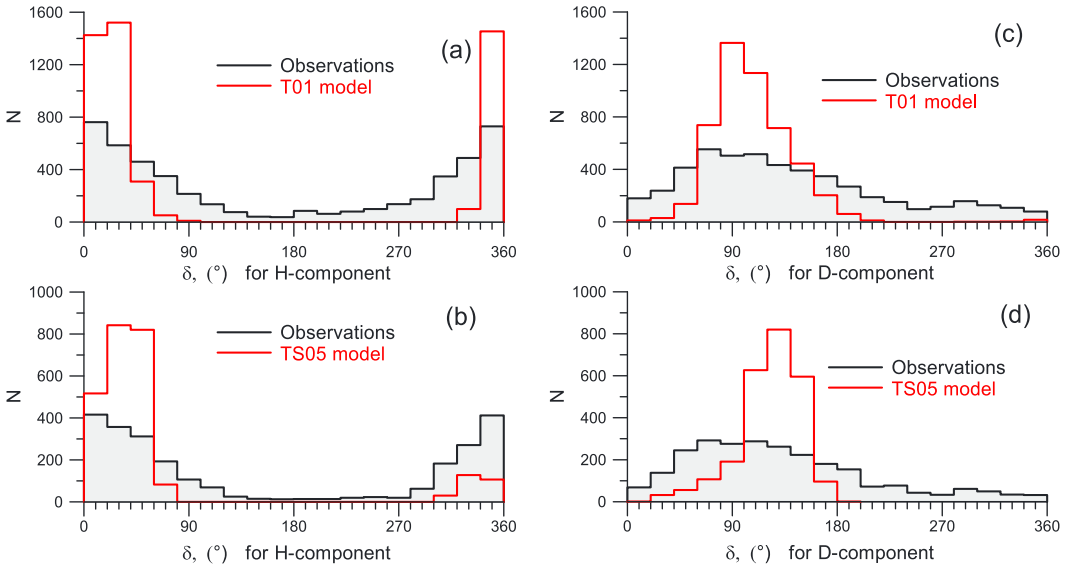

Figure 3. The histograms of the asymmetry phase angle (δ). (a and b) For the *H* component for the T01 and TS05 models, respectively. (c and d) For the *D* component for the T01 and TS05 models, respectively.

that for the observations. At the same time, TS05 shows worse agreement with the peaks of distributions being centered 30–40° to the east from those for the observations. We tried and did not find any meaningful correlation between δ angles computed for the models and observations.

6. Relative Contribution of Current Systems to the Indices

6.1. Case Study, TS05 Model

The results presented in sections 4 and 5 show that the models, on average, reproduce the magnitude and orientation of the local time asymmetry of the ground midlatitude magnetic field. The T01 and TS05 models allow to output the magnetic field of its modules separately (see section 2.1). We use this feature to study the relative contribution of the current systems to the *SYM* and *ASY* indices. For every current system, we computed the contribution to a particular index as described in section 3. The curves with different colors in Figure 4a correspond to the contributions to *SYM-H* index from different current systems of the TS05 model (corresponding figures for T01 model can be found in the supporting information). Figure 4b shows the real *SYM-H* index and the total model index (a sum of the contribution from all systems divided by 0.8). It is seen that the cross-tail current module gives ~−35 nT contribution, and it is the main contributor to *SYM-H* during the main phase and early recovery (other systems give 2 times smaller contributions). Surprisingly, the contribution from region 1 FAC is stronger (~−12 nT) than that from partial ring current module (~−7 nT), but this effect is not seen in the statistical study (see next section).

We also carried out a similar analysis for the *ASY-H* and *ASY-D* indices. Figures 4c and 4d show the *ASY-H* index computed for every model current system separately (in other words, the magnitude of the asymmetry of the current system disturbance field). Figures 4e shows the real *ASY-H* index and the total model index divided by 0.8. The blue and red curves in Figures 4c show the *ASY-H* for region 1 and region 2 magnetic fields, respectively. Their peak values (90–120 nT) are higher than the peak value of the model *ASY-H* index itself (~80 nT). It means that the asymmetries of the R1 and R2 systems compensate each other. It is easy to understand since the asymmetries of these systems have an opposite sense, and these systems produce the magnetic fields of opposite signs, so the total field is smaller than the fields of the R1 and R2 systems. The thick dashed dark blue curve in Figure 4c shows the magnetic field asymmetry amplitude of the total large-scale FAC system (R1 and R2). It can be seen that the asymmetry is much smaller than the asymmetries of each system individually and even smaller than the asymmetry of the partial ring current contribution (green line). Figure 4d shows the contribution from the other systems which can give only a minor contribution to *ASY-H*. The relative contribution of the different systems to the *ASY-D* index is similar to that for *ASY-H*. The graphs for *ASY-D* can be found in the supporting information.

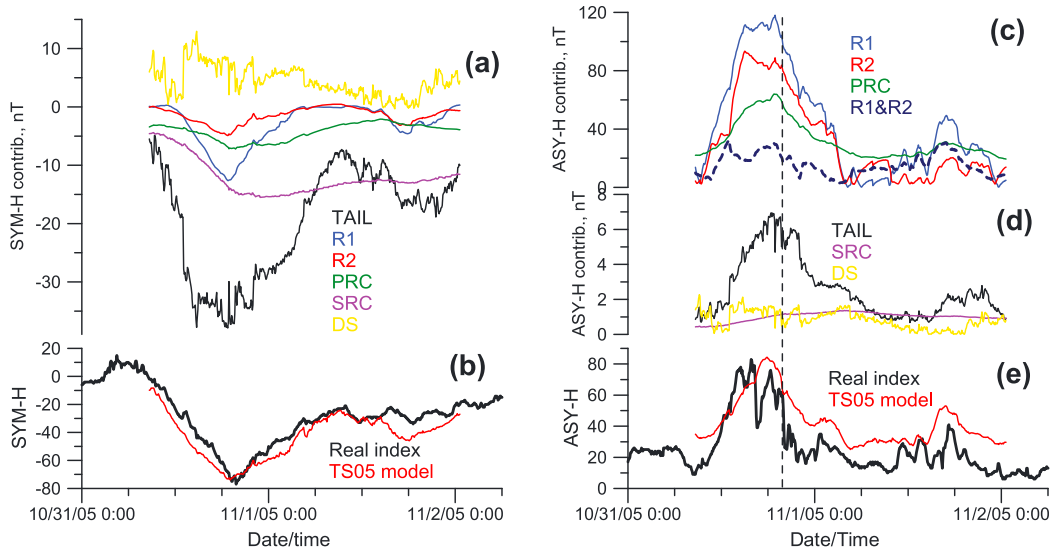

Figure 4. (a) Contribution of the TS05 model current systems to the *SYM-H* index. (b) Real (black) and model (red) *SYM-H* indices. (c) The *ASY-H* contribution of the partial ring current (PRC) and regions 1 and 2 FACs (R1 and R2). (d) *ASY-H* contribution of the tail module, symmetric ring current, and the Earth's dipole shielding field (e) real (black) and model (red) *ASY-H* indices.

6.2. Superposed Epoch Analysis

For Turner's list of the storms (combined CIR- and CME-driven storm list), we carried out a superposed epoch analysis of the relative contribution from the different model modules to the model indices. The time of the real *SYM-H* minimum was used as epoch zero time (t_0) irrespectively of the index analyzed. For every storm, the model index as well as the contributions from the different modules were normalized by the peak value of the model index during the storm (| min(*SYM-H*)| for *SYM-H* and maximum value for the *ASY* indices). After that, these normalized data were binned according their epoch time (15 min bin size). The median value of the superposed model indices and the contributions from different systems were computed for every 15 min bin.

The results of the superposed epoch analysis are shown in Figure 5. The left and right columns are for the T01 and TS05 models, respectively. The bottom panels show the number of storms whose data contributed to the corresponding bins. Figure 5 shows the dynamics of the relative contributions from the model modules to the total model indices. The black thick curves correspond to the total model indices, while the thin curves show contributions from the model modules.

However, Figure 5 shows only average curves, and if the scattering of the separate events relative to the average value is big, our results are not significant. To assess the degree of the scattering, we computed the standard deviation in every time bin for every curve in Figure 5. We use this value as an estimate of the statistical error. The result is shown in Figure 6. The colors and panel order correspond exactly to those in Figure 5.

For easier determination of the module contribution as a fraction of the total model index, we also used another normalization technique. This time, the contributions from the different modules were normalized by the total model index for every moment of time. After that, a binning procedure was applied as described in the previous paragraph. The corresponding curves are shown in Figure 7. That is, a 0.5 value of the vertical axis corresponds to 50% contribution. Note that this percentage is given relative to the total model index and not the real one. Although we will mostly refer to Figure 5, the reader is recommended to check Figure 7 when needed. Figures 5a and 5b show the dynamics of the relative contributions from the model systems to the model *SYM-H* index. The TAIL module is the main contributor during the main phase for both models (black thin curve). The second strongest contributor is the SRC module (magenta), and the third is PRC (green). The Chapman-Ferraro currents shielding Earth's dipole (yellow) give a positive contribution to *SYM-H* which is strongest during the main phase when solar wind dynamic pressure is on average higher. The combined effect from the R1 and R2 modules is very weak.

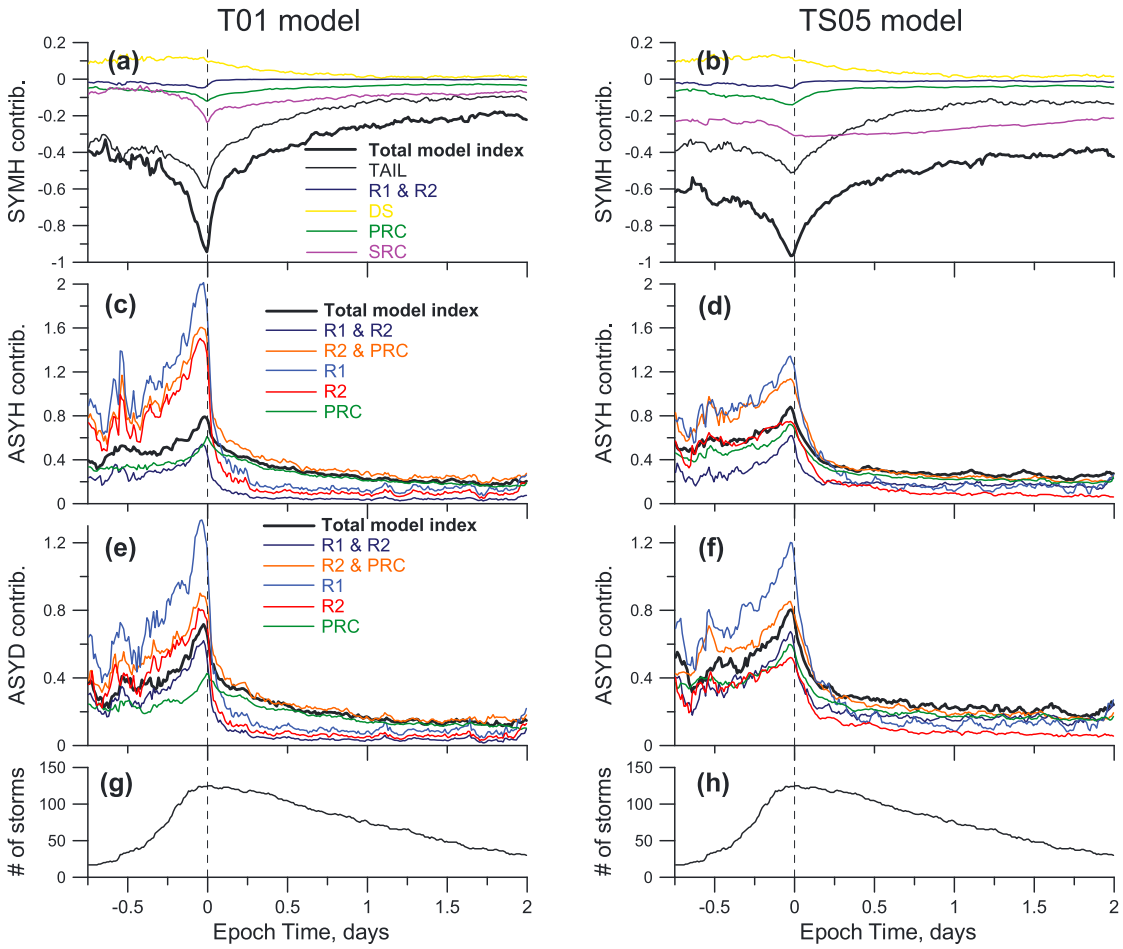

Figure 5. (a–h) Superposed epoch analysis of the normalized contribution of the different model current systems to *SYM-H*, *ASY-H*, and *ASY-D* indices. Figures 5a, 5c, 5e, and 5g and Figures 5b, 5d, 5f, and 5h correspond to the T01 and TS05 models, respectively. Thick black curves correspond to the normalized total model index, while thin curves show the contribution of different model modules.

There is a prominent difference between the two models. Note that the contribution of T01 SRC reaches ~20% only by the very end of the main phase while TS05 SRC shows ~30% throughout the main phase. The difference is even more prominent for the recovery phase. Although the fraction of the SRC contribution relative to other systems increases during the recovery phase in both models, the T01 SRC contribution is always less than that for the TAIL module while the TS05 SRC contribution becomes larger than that from the TAIL module ~6 h after the *SYM-H* minimum and attains ~50% of the total model index. Similar analysis was carried out in *Tsyganenko and Sitnov* [2005] for a few storms using TS05. Our Figure 5b mostly reproduces their Figure 6. Note, however, that the results of *Tsyganenko and Sitnov* [2005] were obtained before the bug in the TS05 SRC module, which produced incorrect field values in the near-Earth region, was fixed in 2006. This can explain the somewhat higher contribution from SRC (in comparison to our result) in their Figures 4 and 5.

Figures 6a and 6b show that the statistical error for the contributions from the separate current systems does not exceed a value of 0.2 and is somewhat lower during a recovery phase. A comparison of Figures 5a and 5b and Figures 6a and 6b shows that all results discussed in two previous paragraphs are statistically significant.

Figures 5c and 5d and Figures 5e and 5f show the dynamics of the asymmetries of the *H* and *D* component disturbances from the model systems in comparison to model *ASY-H* and *ASY-D* indices, respectively. Only asymmetries of the R1, R2, and PRC systems are shown since the asymmetries of the remaining systems are less than 10% of the model index. The asymmetries of all aforementioned systems peak at or a bit earlier than the *SYM-H* minimum. It can be seen that R1 module gives the largest asymmetry (blue curve) which

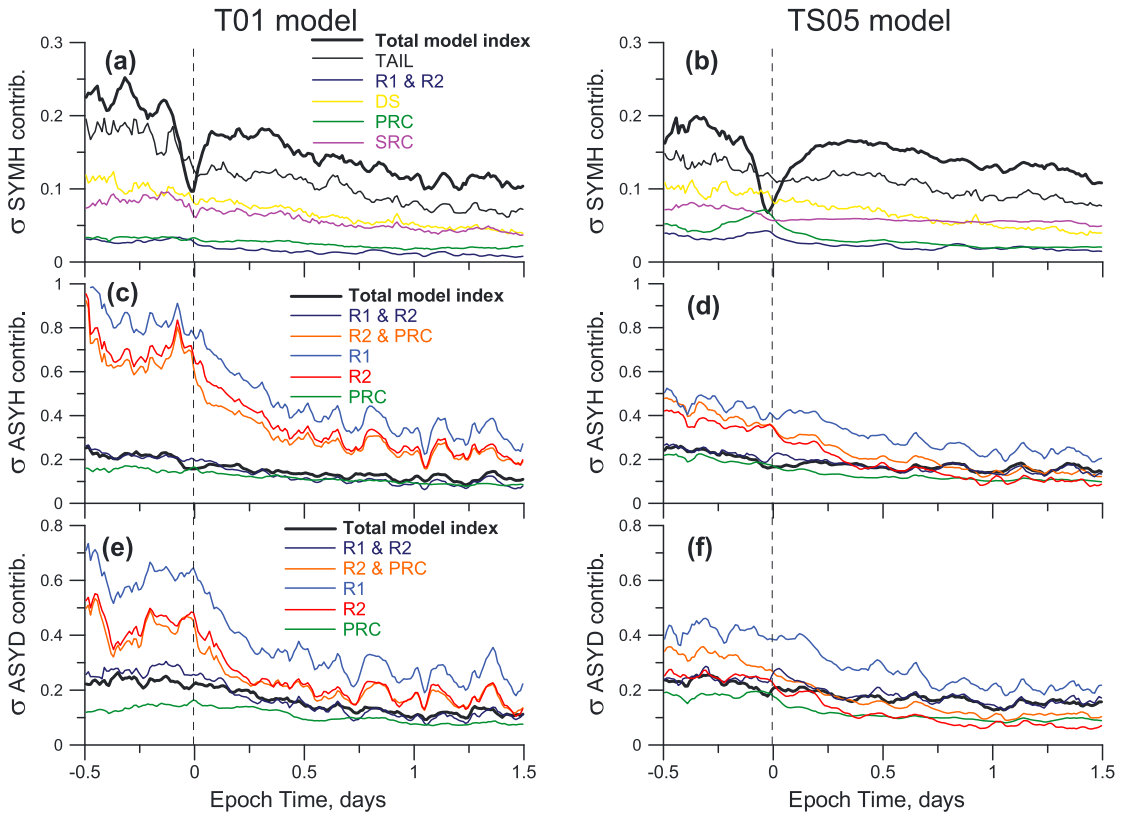

Figure 6. (a–f) Standard deviations of the superposed curves inside time bins. Figures 6a, 6c, and 6e and Figures 6b, 6d, 6f correspond to the T01 and TS05 models, respectively.

is much larger than the asymmetry of the total model field during the main phase. However, the R1 field is compensated by the field of the R2 module (red curve), so that the resulting asymmetry of the whole R1/R2 system (dark blue curve) is smaller than the total model *ASY* indices. It should be noted that magnitudes of the R1 and R2 asymmetries of the T01 model are approximately 2 times larger than those for the TS05 model during the main phase. At the same time, the asymmetries of the whole R1/R2 system for these two models are comparable. This difference is likely a result of the simple linear dependence of the T01 R1 and R2 FAC intensity on driving parameters while a more advanced nonlinear dependence is utilized in TS05. It is known that the large-scale FACs tend to saturate during storms [*Tsyganenko and Sitnov*, 2005; *Anderson and Korth*, 2007]. At the same time, T01 employs a linear form FAC dependence on driving parameters and cannot describe the effects of saturation, therefore overestimating the FAC intensity.

Figures 6c–6f show that the statistical error for the contributions to *ASY* indices from the R1 and R2 current systems can be as large as 0.9 (for the T01 model R1 *ASY-H* contribution during the main phase). It is larger or comparable to the difference between the contributions from these systems. However, we compared the contributions from the R1 and R2 systems and also from the R1 and combined R2 and PRC systems for the individual events. It was found that the contribution from the R1 system was larger than that from the R2 system for more than 90% of events during the main phase. The contribution from R1 exceeded that from the combined R2 and PRC system for more than 70% of events during the main phase. The results prove that the order of the curves in Figures 5c–5f is statistically significant.

There is a difference of PRC asymmetry behavior shown by the two models. While both models show the increase of PRC asymmetry during the main phase and decrease during the recovery phase, the ratio of the PRC asymmetry to the total model index for TS05 model is nearly constant (Figures 7d and 7f). At the same time, the magnitude of the T01 PRC asymmetry relative to the total model index increases during recovery phase (it is especially obvious for the *D* component).

Since the R2 and PRC current systems occupy approximately the same region and are driven by the same physical mechanism, we also show the asymmetry of the combined R2/PRC system (orange curve). It is

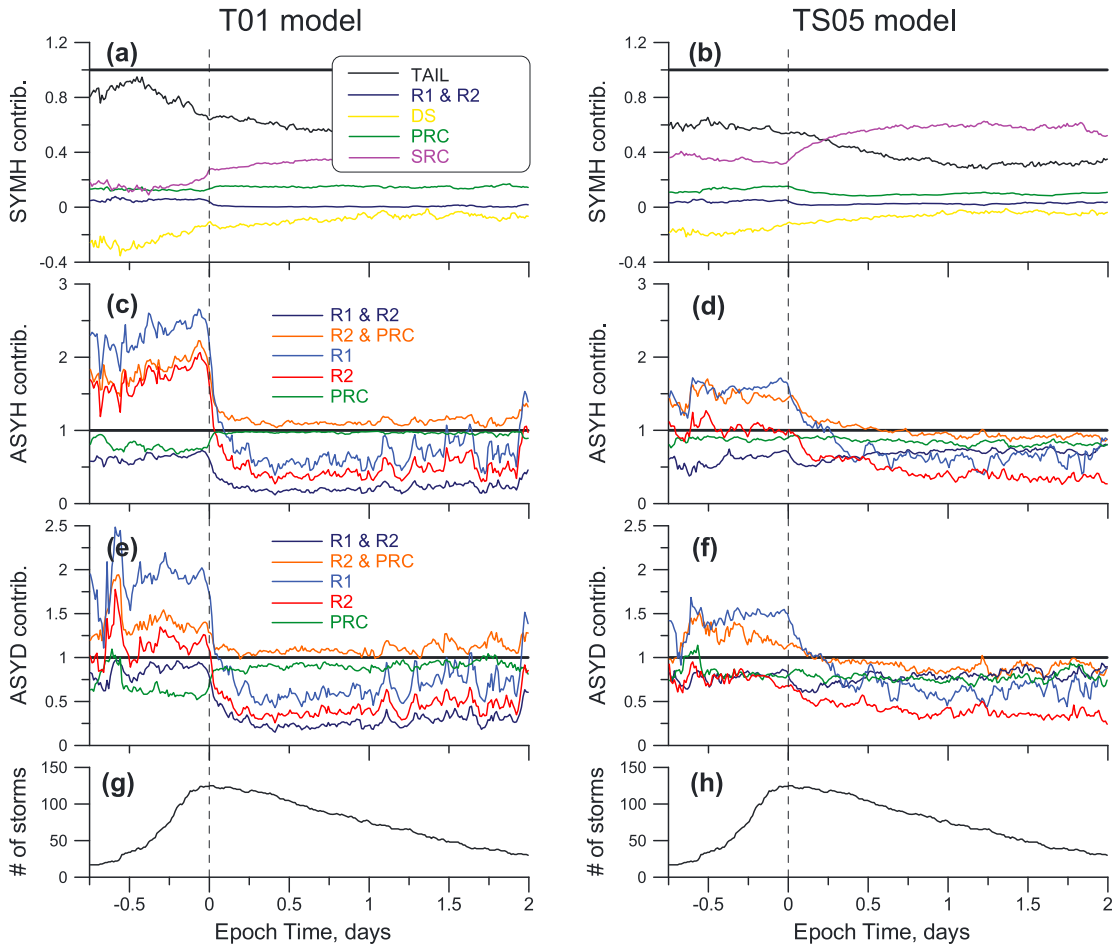

Figure 7. The same curves as in Figure 5 but normalized by the total model indices values for every bin. The vertical axis shows the asymmetry of the systems as a fraction of the total model index.

shown that the main contributors to the model *ASY* indices are the R1, R2, and PRC modules. It can be seen that the combined PRC and R2 system is the major contributor to the *ASY* indices during the recovery phase. In contrast, during the main phase the asymmetry of the R1 system is stronger, though the asymmetry of the PRC and R2 systems cannot be totally neglected. Note also that while the asymmetry of the combined PRC and R2 system for the TS05 model is much larger than the asymmetry of the R2 system alone, these asymmetries are comparable for the T01 model. We speculate that such a difference is due to the presence of the second-order azimuthal harmonic in the representation of the T01 R2 module (see Table 1). This feature allows the T01 R2 module to describe the partial ring current concentrated totally on the nightside and centered at midnight. Thus, the T01 PRC module must only describe the additional effect of the shift of the PRC center from midnight toward dusk. In contrast, the TS05 PRC module has to describe both of these effects. It should be noted that the magnetic field from the R1 and R2 FAC on the ground at midlatitudes depends not only on current system intensity but also on their geometry, particularly on the latitude of the ionospheric foot point of the system. The equatorward shift of the R1 and R2 system in the T01 model is proportional to the G_2 parameter, while it is proportional to the *SYM-H* index in the TS05 model (see section 2.2 for details). This difference also can be a cause of the difference of the R1 and R2 asymmetries for these two models.

We also performed the same analysis separately for CIR- and CME-driven storms as well as for strong (-250 nT $<$ min *SYM-H* $<$ -100 nT) and moderate (-100 nT$<$ min *SYM-H* $<$ -50 nT) storms. The corresponding figures can be found in the supporting information. The difference between the results obtained for these two subsets were smaller than the difference between the two models.

Since a minimum of *SYM-H* index was chosen as a reference time, it is natural that the superposed *SYM-H* curves reveal quite sharp minima (Figures 5a and 5b). Note that the T01 superposed *SYM-H* curve shows

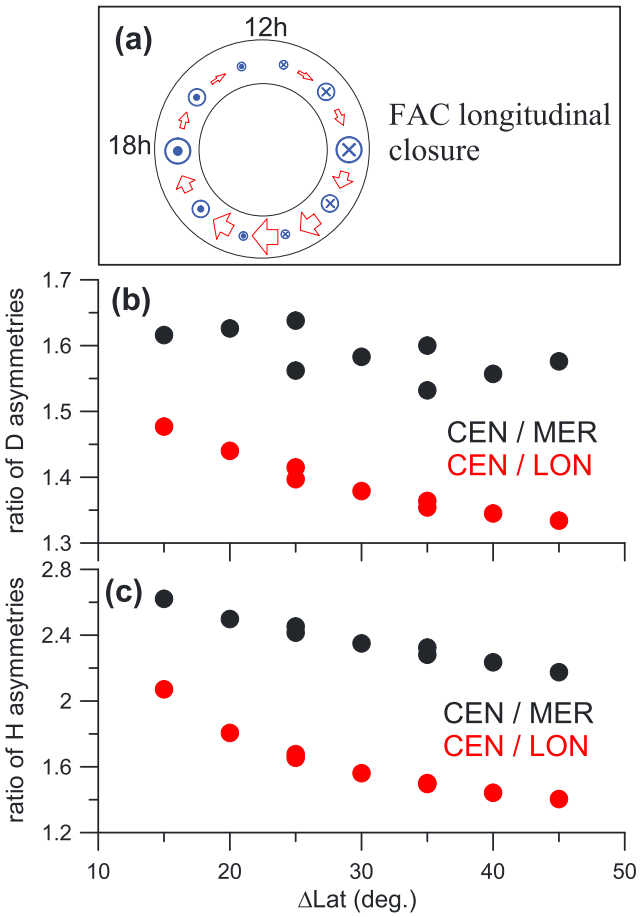

Figure 8. (a) Illustration of the longitudinal closure of the idealized FAC system. (b) Ratio of the *D* component asymmetries computed for different closure paths. (c) The same ratio for the *H* component. ΔLat is the difference between latitude of the FACs and latitude of the virtual observatories.

sharper a minimum than the TS05 curve. It is due to the fact that the T01 current systems making the main contribution to the *SYM-H* index (TAIL and SRC modules) are directly parameterized by the *SYM-H* index while these modules are controlled by solar wind parameters in TS05.

6.3. The Effect of the Unrealistic Model FAC Closure

We performed a numerical test to check how the unrealistic closure of the model FACs through the Earth's center can affect our model/real *ASY* indices comparison. We computed the ground magnetic effect of an idealized FAC system for different configurations of the closure currents. Our idealized FAC system was based on the schema of the R1/R2 current closure presented in Figure 2 of *Baumjohann* [1983]. According to the schema, the R1 and R2 FACs close entirely within the auroral oval with no closure currents flowing over the polar cap. Some parts of the R1 and R2 FACs close via the nearly meridional Pedersen currents, and the residual unbalanced (net) currents close via the Hall electrojets in the longitudinal direction. We consider the contributions from these two components of ionospheric closure currents and field-aligned segment of current separately. Since the distance between the R1 and R2 FAC sheets is only a few degrees in latitude, we expect that the contribution from Pedersen/meridional closure currents is small in comparison to the contribution from the extended field-aligned and longitudinal closure currents. Using Biot-Savart integration of the R1-like FAC system, we computed the magnetic field on the ground. It was assumed that FAC flows along dipole field lines in an infinitely thin axially symmetric surface crossing the ionosphere at a constant geomagnetic latitude in the Northern and Southern Hemispheres. The magnetic field was computed at the points at fixed latitude in the Northern Hemisphere distributed evenly over local time. For simplicity, we consider a symmetric configuration with no dipole tilt. The FAC current intensity varies as a sine function of MLT. Three different integration schemes represent three scenarios of the FAC closure. The first integration is performed along the dipole filed lines from the equatorial part to ionospheric altitudes ($h = 120$ km). It simulates FAC system with meridional closure current (referred to as MER; The meridional ionospheric closure current contribution is neglected). The second integration was performed from the equatorial part to the Earth's center (imitation of the magnetospheric model closure, referred to as CEN). For the third integration, every elementary current flow line was integrated from the equatorial part to the ionosphere and then along the longitude over nightside to the symmetric point on the other flank (imitation of the system with longitudinal closure, referred to as LON). Figure 8a shows the schema of this longitudinal closure. In all three cases, we neglected the contribution from the closure currents in the equatorial magnetosphere. In fact, the schema of *Baumjohann* [1983] suggests the closure between the R1 and R2 systems while we compute the effect from the azimuthal closure of the single R1-like system. Yet our closure schema can be used for a rough estimation of the model inaccuracy. The asymmetry of the *D* and *H* components were computed for all

three systems as a difference between maximum and minimum values among all local time sectors. A few runs were performed for different values of the FAC ionospheric foot point latitudes (55–65°, the range for the storm time FAC [*Anderson et al.*, 2005; *Anderson and Korth*, 2007]) and different latitudes of the virtual observatories (20–30°, see Table 2). It turned out that the results of all runs could be organized using one parameter: a distance in latitude between the FAC and virtual observatories.

Figures 8b and 8c show the ratios of the asymmetry obtained for closure through the Earth's center to asymmetries for meridional (black symbols) and longitudinal (red symbols) closures. This ratio is a rough estimate of the effect of the unrealistic closure of the model currents (in other words, the model indices should be divided by these values when compared to the real indices). Figures 8b and 8c correspond to *D* and *H* component asymmetries. The horizontal axis shows the distance in latitude between the FAC and virtual observatories. The red and black symbols represent the high and low estimates of the possible effect of the unrealistic FAC closure. It can be seen that the ratio is higher for the *H* component (1.4–2.6) while it is in within 1.3–1.6 for the *D* component. These corrections can explain somewhat high values of the model to the real index ratio presented in Table 3. However, they highlight disagreement for the TS05 *ASY-D* index.

6.4. Brief Summary of the Section

Although T01 and TS05 show a bit different results, both models are in agreement about the key results. (1) The TAIL module gives the main contribution to *SYM-H* during the main phase. (2) The relative contribution of the SRC module to *SYM-H* starts to increase a bit prior or just after *SYM-H* minimum (the two models differ about whether the SRC becomes the dominant contributor during the recovery phase). (3) Only modules having closure current via the ionosphere can contribute to the *ASY* indices. (4) There is not much difference between the *ASY-H* and *ASY-D* indices. (5) The R1 module is the main contributor to the *ASY* indices during the main phase. Though, the R2 and PRC contributions are not negligible.

7. Discussion

The results presented in sections 4 and 5 show that the empirical magnetospheric models T01, TS05, and TS07 can reproduce the average variations of the real midlatitude indices. The best correlation between the real index and model estimate (r∼0.8–0.9) was found for *SYM-H* index while correlation r∼0.6–0.8 and r∼0.5–0.7 were found for *ASY-H* and *ASY-D*, respectively. For reference, we computed the correlation coefficients between the real indices and a few known solar wind driving parameters (we used the parameters tested by *Newell et al.* [2007] as well as the empirical formula for polar cap potential [*Boyle et al.*, 1997]) for Turner's list of the storms. The best correlation was found with the Boyle's formula, namely, $r = 0.6$ and $r = 0.63$ for *ASY-H* and *SYM-D*, respectively.

Although TS07 addresses the dusk-dawn asymmetry in a more advanced way than T01 and TS05, it shows a bit worse correlation. The explanation is that the main advantage of the TS07 model, higher spatial resolution of the current systems in equatorial plane, is not crucial for description of the ground magnetic disturbance. On the other hand, the simplified parametrization of TS07, which includes only three parameters averaged over a long period, might reduce the model's ability to reproduce ground indices. However, the fact that TS05 and T01 show better correlation with real indices than TS07 proves that no essential details are missed due to any limitation of the mathematical constraint of TS05 and T01.

However, the high correlation of model and real indices just shows that they vary in a similar way but does not give information about accuracy of the model. On the other hand, the analysis of the residual is complicated since the contribution of the ground-induced currents are never accurately known. This contribution is different for various stations and phases of the storm and can be estimated roughly as 25% [*Häkkinen et al.*, 2002; *Langel and Estes*, 1985]. The comparison of the peak values of the model and real *SYM-H* index (see Table 3) shows good agreement with this estimate (25% contribution of induced currents in the Earth corresponds to the ratio of the model to real index ∼0.8). However, the agreement is worse for the *ASY* indices. This can be explained by interference from sudden solar wind dynamic pressure enhancements. These pulses can lead to an increase of the low-latitude and midlatitude asymmetry [*Shi et al.*, 2005, 2006], and the models do not incorporate this effect [*Shi et al.*, 2008a]. In addition, unrealistic closure of the FAC in the models can worsen the correlations for *ASY* indices.

Campbell [2004] claimed that ionospheric currents could be the main source of the midlatitude and low-latitude *H* component disturbance during storms. However, we found that the magnetospheric models

generally reproduce the *SYM-H* and *ASY* indices with an accuracy of ~17% and < 40%, respectively (section 4). We are inclined to think that these moderate discrepancies are mostly due to the model predefined structure and limited resolution rather than due to the ionospheric current effect.

The analysis of the event presented in section 4.1 demonstrates that the model *SYM-H* index is very close to the real one (particulary for the T01 model). On the other hand, the models can only reproduce long-term variations of the *ASY* indices, often being inaccurate on the time scales less than 3 h.

Although the models often cannot give an accurate description of the midlatitude indices for a particular storm, they show reasonable agreement after averaging. Encouraged by this result, we use the model for statistical analysis of the contributions from the various current systems to the midlatitude indices. The superposed epoch analysis of the contribution from the model systems to the *SYM-H* index mostly confirmed the results of previous studies [*Tsyganenko and Sitnov*, 2005; *Ganushkina et al.*, 2012b]. These studies showed that the tail current module gives the largest contribution to *SYM-H* during the main phase. However, such an approach can lead to a confusion [*Liemohn et al.*, 2011; *Ganushkina et al.*, 2012b]. A few modules of the T01 and TS05 models, namely, PRC, R2, and inner TAIL module, overlap in the nightside inner magnetosphere so that the resulting current flows along the streamlines which can be completely different from those of the TAIL module current alone. Using the TS05 model, *Ganushkina et al.* [2012b] showed that the streamlines of the total model current traced from the region of the strongest TAIL module current closed through the ionosphere, though the PRC and R2 modules gave a modest contribution to *SYM-H* for that event. However, this precaution is not valid for the SRC module contribution since it occupies the innermost region of the magnetosphere and does not overlap with other systems. The contribution to *SYM-H* from the SRC module shows behavior consistent with the conventional storm scenario: gradual increase during the main phase and slow decay during the recovery phase.

Fukushima and Kamide [1973] showed that the ionospheric closure current and the magnetospheric closure of the partial ring current do not make a significant contribution to the *H* component longitudinal asymmetry. We indeed found that only current systems closing via field-aligned currents can make a significant contribution to the *ASY* indices. Although the *ASY-H* index is often considered as an indicator of the PRC strength, our results show that the region 1 currents produce the largest asymmetry of the *D* and *H* components during the main phase. It means that the *ASY* indices reflect the degree of mutual cancellation between R1 system on one part and R2 and PRC systems on the other part. This result is in agreement with conclusions of *Harel et al.* [1981] and *Iyemori* [1990]. The authors suggested that there was a net (unbalanced) current at noon and at midnight. However, it should be noted that the geometry of the model's R1 and R2 FACs does not allow of net current concentrated at noon or at midnight. The R1 and R2 modules are purely odd functions with respect to the noon-midnight meridian, and the only system which can produce current at the noon meridian is the PRC.

Our results resolve some of inconsistencies of the "substorm-controlled" scenario of the geomagnetic storms mentioned in *Iyemori and Rao* [1996] and *Maltsev* [2004]. We have shown that both the R1 and R2 (and PRC) systems produce comparable magnetic field asymmetry at midlatitudes (R1 usually produces stronger asymmetry than R2 despite its location at higher latitudes). It explains why *ASY-H* shows better correlation with southward IMF than with the *AL* index [*Clauer et al.*, 1983].

The contribution of the tail current to *SYM-H* computed in section 6.2 is probably overestimated [see *Ganushkina et al.*, 2012b], and the real contribution can be closer to the estimate of *Turner et al.* [2000]. The enhanced convection during the main phase pumps magnetic flux in the lobes and strengthens the tail current as well as moves it closer to the Earth. Although the substorms might not happen at this phase, the increased cross-tail current leads to a *SYM-H* dip. This mechanism explains the good correlation of *SYM-H* decreases with southward IMF.

8. Conclusions

In sections 4 and 5 we found a good agreement between the *SYM* and *ASY* indices computed using the magnetospheric empirical models T01 [*Tsyganenko*, 2002a] and TS05 [*Tsyganenko and Sitnov*, 2005] and real indices. These results together with the model modular structure allow us to use these models for separation of the contributions from different current systems. We carried out the statistical analysis of the model indices computed for ~200 storms which resulted in the following conclusions:

1. The good agreement between the indices computed using magnetospheric models and real ones indicates that purely ionospheric current systems, on average, give modest contribution to these indices (< 17% to *SYM-H* and < 40% to *ASY-H* and *ASY-D*).
2. Although it was found that the cross-tail current gives the dominant contribution to the *SYM-H* index during the main phase, this result should be taken with a precaution. It should be remembered that the model region 2, partial ring current, and cross-tail current systems are not spatially demarcated (the systems are overlapped in the vicinity of geostationary orbit).
3. The relative contribution from the symmetric ring current to *SYM-H* starts to increase a bit prior or just after *SYM-H* minimum and attains its maximum during the recovery phase.
4. Only current systems which close via the ionosphere give a significant contribution to the *ASY-H* and *ASY-D* indices. These systems are the partial ring current and FAC regions 1 and 2.
5. The region 1 FAC is the main contributor to the *ASY-H* and *ASY-D* indices during the main phase, though region 2 FAC and partial ring current contributions are not negligible.
6. The aforementioned findings naturally resolve the long-debated inconsistencies of the substorm-controlled geomagnetic storm scenario.

Acknowledgments

The authors acknowledge the Kyoto World Data Center for Geomagnetism. The results presented in this paper rely on data collected at magnetic observatories. We thank the national institutes that support them and INTERMAGNET for promoting high standards of magnetic observatory practice (www.intermagnet.org). Work by S. Dubyagin was supported by an Academy of Finland grant. Work by N. Ganushkina was partly supported by NASA, NSF, and Academy of Finland grants. Work by M. Liemohn was supported by various NASA and NSF grants.

Michael Balikhin thanks Vladimir Kalegaev and another reviewer for their assistance in evaluating this paper.

References

Akasofu, S.-I., and S. Chapman (1964), On the asymmetric development of magnetic storm fields in low and middle latitudes, *Planet. Space Sci.*, *12*(6), 607–626, doi:10.1016/0032-0633(64)90008-X.

Alexeev, I. I., E. S. Belenkaya, V. V. Kalegaev, Y. I. Feldstein, and A. Grafe (1996), Magnetic storms and magnetotail currents, *J. Geophys. Res.*, *101*(A4), 7737–7747, doi:10.1029/95JA03509.

Alexeev, I. I., V. V. Kalegaev, E. S. Belenkaya, S. Y. Bobrovnikov, Y. I. Feldstein, and L. I. Gromova (2001), Dynamic model of the magnetosphere: Case study for January 9–12, 1997, *J. Geophys. Res.*, *106*(A11), 25,683–25,693, doi:10.1029/2001JA900057.

Anderson, B. J., S.-I. Ohtani, H. Korth, and A. Ukhorskiy (2005), Storm time dawn-dusk asymmetry of the large-scale Birkeland currents, *J. Geophys. Res.*, *110*, A12220, doi:10.1029/2005JA011246.

Anderson, B. J., and H. Korth (2007), Saturation of global field aligned currents observed during storms by the Iridium satellite constellation, *J. Atmos. Sol. Terr. Phys.*, *69*, 166–169, doi:10.1016/j.jastp.2006.06.013.

Baumjohann, W. (1983), Ionospheric and field-aligned current systems in the auroral zone: A concise review, *Adv. Space Res.*, *2*(10), 55–62, doi:10.1016/0273-1177(82)90363-5.

Bogott, F. H., and F. S. Mozer (1973), ATS-5 observations of energetic proton injection, *J. Geophys. Res.*, *78*(34), 8113–8118, doi:10.1029/JA078i034p08113.

Borovsky, J. E., and M. H. Denton (2006), Differences between CME-driven storms and CIR-driven storms, *J. Geophys. Res.*, *111*, A07S08, doi:10.1029/2005JA011447.

Boyle, C. B., P. H. Reiff, and M. R. Hairston (1997), Empirical polar cap potentials, *J. Geophys. Res.*, *102*(A1), 111–125, doi:10.1029/96JA01742.

Cahill, L. J., Jr. (1966), Inflation of the inner magnetosphere during a magnetic storm, *J. Geophys. Res.*, *71*(19), 4505–4519, doi:10.1029/JZ071i019p04505.

Campbell, W. H. (1996), Geomagnetic storms, the Dst ring-current myth and lognormal distributions, *J. Atmos. Terr. Phys.*, *58*, 1171–1187, doi:10.1016/0021-9169(95)00103-4.

Campbell, W. H. (2004), Failure of Dst index fields to represent a ring current, *Space Weather*, *2*, S08002, doi:10.1029/2003SW000041.

Campbell, W. H. (2008), Comment on "Unraveling the causes of radiation belt enhancements," *Eos Trans. AGU*, *89*, 379, doi:10.1029/2008EO400006.

Clauer, C. R., and R. L. McPherron (1980), The relative importance of the interplanetary electric field and magnetospheric substorms on partial ring current development, *J. Geophys. Res.*, *85*(A12), 6747–6759, doi:10.1029/JA085iA12p06747.

Clauer, C. R., R. L. McPherron, and C. Searls (1983), Solar wind control of the low-latitude asymmetric magnetic disturbance field, *J. Geophys. Res.*, *88*(A3), 2123–2130, doi:10.1029/JA088iA03p02123.

Crooker, N. U., and G. L. Siscoe (1971), A study of the geomagnetic disturbance field asymmetry, *Radio Sci.*, *6*(4), 495–501, doi:10.1029/RS006i004p00495.

Crooker, N. U., and G. L. Siscoe (1981), Birkeland currents as the cause of the low-latitude asymmetric disturbance field, *J. Geophys. Res.*, *86*(A13), 11,201–11,210, doi:10.1029/JA086iA13p11201.

Cummings, W. D. (1966), Asymmetric ring currents and the low-latitude disturbance daily variation, *J. Geophys. Res.*, *71*(19), 4495–4503, doi:10.1029/JZ071i019p04495.

Dessler, A. J., and E. N. Parker (1959), Hydromagnetic theory of geomagnetic storms, *J. Geophys. Res.*, *64*(12), 2239–2252, doi:10.1029/JZ064i012p02239.

Dremukhina, L. A., Y. I. Feldstein, I. I. Alexeev, V. V. Kalegaev, and M. E. Greenspan (1999), Structure of the magnetospheric magnetic field during magnetic storms, *J. Geophys. Res.*, *104*(A12), 28,351–28,360, doi:10.1029/1999JA900261.

Friedrich, E., G. Rostoker, M. G. Connors, and R. L. McPherron (1999), Influence of the substorm current wedge on the Dst index, *J. Geophys. Res.*, *104*(A3), 4567–4575, doi:10.1029/1998JA900096.

Fukushima, N., and Y. Kamide (1973), Partial ring current models for worldwide geomagnetic disturbances, *Rev. Geophys.*, *11*(4), 795–853, doi:10.1029/RG011i004p00795.

Ganushkina, N. Yu., T. I. Pulkkinen, M. V. Kubyshkina, H. J. Singer, and C. T. Russell (2004), Long-term evolution of magnetospheric current systems during storms, *Ann. Geophys.*, *22*, 1317–1334, doi:10.5194/angeo-22-1317-2004.

Ganushkina, N. Yu., M. W. Liemohn, and T. I. Pulkkinen (2012a), Storm-time ring current: Model-dependent results, *Ann. Geophys.*, *30*, 177–202, doi:10.5194/angeo-30-177-2012.

Ganushkina, N. Y., S. Dubyagin, M. Kubyshkina, M. Liemohn, and A. Runov (2012b), Inner magnetosphere currents during the CIR/HSS storm on July 21–23, 2009, *J. Geophys. Res.*, *117*, A00L04, doi:10.1029/2011JA017393.

Gonzalez, W. D., J. A. Joselyn, Y. Kamide, H. W. Kroehl, G. Rostoker, B. T. Tsurutani, and V. M. Vasyliunas (1994), What is a geomagnetic storm?, *J. Geophys. Res.*, *99*(A4), 5771–5792, doi:10.1029/93JA02867.

Häkkinen, L. V. T., T. I. Pulkkinen, H. Nevanlinna, R. J. Pirjola, and E. I. Tanskanen (2002), Effects of induced currents on Dst and on magnetic variations at midlatitude stations, *J. Geophys. Res.*, *107*(A1), SMP 7-1–SMP 7-8, doi:10.1029/2001JA900130.

Harel, M., R. A. Wolf, R. W. Spiro, P. H. Reiff, C.-K. Chen, W. J. Burke, F. J. Rich, and M. Smiddy (1981), Quantitative simulation of a magnetospheric substorm 2. Comparison with observations, *J. Geophys. Res.*, *86*(A4), 2242–2260, doi:10.1029/JA086iA04p02242.

Huang, C.-L., H. E. Spence, H. J. Singer, and N. A. Tsyganenko (2008), A quantitative assessment of empirical magnetic field models at geosynchronous orbit during magnetic storms, *J. Geophys. Res.*, *113*, A04208, doi:10.1029/2007JA012623.

Iyemori, T. (1990), Storm-time magnetospheric currents inferred from mid-latitude geomagnetic field variations, *J. Geomag. Geoelectr.*, *42*, 1249–1265.

Iyemori, T., and D. R. K. Rao (1996), Decay of the Dst field of geomagnetic disturbance after substorm onset and its implication to storm-substorm relation, *Ann. Geophys.*, *14*, 608–618, doi:10.1007/s00585-996-0608-3.

Iyemori, T. (2010), Mid-latitude geomagnetic indices "ASY" and "SYM" for 2009 (Provisional). [Available at http://wdc.kugi.kyoto-u.ac.jp/aeasy/asy.pdf.]

Kalegaev, V. V., N. Y. Ganushkina, T. I. Pulkkinen, M. V. Kubyshkina, H. J. Singer, and C. T. Russell (2005), Relation between the ring current and the tail current during magnetic storms, *Ann. Geophys.*, *23*, 523–533, doi:10.5194/angeo-23-523-2005.

Kamide, Y. (1992), Is substorm occurrence a necessary condition for a magnetic storm?, *J. Geomag. Geoelectr.*, *44*, 109–117.

Katus, R. M., and M. W. Liemohn (2013), Similarities and differences in low-to middle-latitude geomagnetic indices, *J. Geophys. Res. Space Physics*, *118*, 5149–5156, doi:10.1002/jgra.50501.

Kawasaki, K., and S.-I. Akasofu (1971), Low-latitude DS component of geomagnetic storm field, *J. Geophys. Res.*, *76*(10), 2396–2405, doi:10.1029/JA076i010p02396.

Langel, R. A., and R. H. Estes (1985), Large-scale, near-field magnetic fields from external sources and the corresponding induced internal field, *J. Geophys. Res.*, *90*(B3), 2487–2494, doi:10.1029/JB090iB03p02487.

Liemohn, M. W. (2003), Yet another caveat to using the Dessler-Parker-Sckopke relation, *J. Geophys. Res.*, *108*(A6), 1251, doi:10.1029/2003JA009839.

Liemohn, M. W., and A. A. Chan (2008), Reply to comment on "Unraveling the causes of radiation belt enhancements," *Eos Trans. AGU*, *89*(40), 379, doi:10.1029/2008EO400007.

Liemohn, M. W., J. U. Kozyra, M. F. Thomsen, J. L. Roeder, G. Lu, J. E. Borovsky, and T. E. Cayton (2001), Dominant role of the asymmetric ring current in producing the stormtime Dst, *J. Geophys. Res.*, *106*, 10,883–10,904, doi:10.1029/2000JA000326.

Liemohn, M. W., D. L. De Zeeuw, R. Ilie, and N. Y. Ganushkina (2011), Deciphering magnetospheric cross-field currents, *Geophys. Res. Lett.*, *38*, L20106, doi:10.1029/2011GL049611.

Maltsev, Y. P. (2004), Points of controversy in the study of magnetic storms, *Space Sci. Rev.*, *110*, 227–277, doi:10.1023/B:SPAC.0000023410.77752.30.

Munsami, V. (2000), Determination of the effects of substorms on the storm-time ring current using neural networks, *J. Geophys. Res.*, *105*(A12), 27,833–27,840, doi:10.1029/2000JA000041.

Newell, P. T., T. Sotirelis, K. Liou, C.-I. Meng, and F. J. Rich (2007), A nearly universal solar wind-magnetosphere coupling function inferred from 10 magnetospheric state variables, *J. Geophys. Res.*, *112*, A01206, doi:10.1029/2006JA012015.

Ohtani, S., M. Nosé, G. Rostoker, H. Singer, A. T. Y. Lui, and M. Nakamura (2001), Storm-substorm relationship: Contribution of the tail current to Dst, *J. Geophys. Res.*, *106*(A10), 21,199–21,209, doi:10.1029/2000JA000400.

Russell, C. T., R. L. McPherron, and R. K. Burton (1974), On the cause of geomagnetic storms, *J. Geophys. Res.*, *79*(7), 1105–1109, doi:10.1029/JA079i007p01105.

Sckopke, N. (1966), A general relation between the energy of trapped particles and the disturbance field near the Earth, *J. Geophys. Res.*, *71*(13), 3125–3130, doi:10.1029/JZ071i013p03125.

Shi, Y., E. Zesta, L. R. Lyons, A. Boudouridis, K. Yumoto, and K. Kitamura (2005), Effect of solar wind pressure enhancements on storm time ring current asymmetry, *J. Geophys. Res.*, *110*, A10205, doi:10.1029/2005JA011019.

Shi, Y., E. Zesta, L. R. Lyons, K. Yumoto, and K. Kitamura (2006), Statistical study of effect of solar wind dynamic pressure enhancements on dawn-to-dusk ring current asymmetry, *J. Geophys. Res.*, *111*, A10216, doi:10.1029/2005JA011532.

Shi, Y., E. Zesta, and L. R. Lyons (2008a), Modeling magnetospheric current response to solar wind dynamic pressure enhancements during magnetic storms: 1. Methodology and results of the 25 September 1998 peak main phase case, *J. Geophys. Res.*, *113*, A10218, doi:10.1029/2008JA013111.

Shi, Y., E. Zesta, and L. R. Lyons (2008b), Modeling magnetospheric current response to solar wind dynamic pressure enhancements during magnetic storms: 2. Application to different storm phases, *J. Geophys. Res.*, *113*, A10219, doi:10.1029/2008JA013420.

Sitnov, M. I., N. A. Tsyganenko, A. Y. Ukhorskiy, and P. C. Brandt (2008), Dynamical data-based modeling of the storm-time geomagnetic field with enhanced spatial resolution, *J. Geophys. Res.*, *113*, A07218, doi:10.1029/2007JA013003.

Sitnov, M. I., N. A. Tsyganenko, A. Y. Ukhorskiy, B. J. Anderson, H. Korth, A. T. Y. Lui, and P. C. Brandt (2010), Empirical modeling of a CIR-driven magnetic storm, *J. Geophys. Res.*, *115*, A07231, doi:10.1029/2009JA015169.

Suigura, M. (1964), Hourly values of the equatorial Dst for IGY, in *Annals of the International Geophysical Year*, vol. 35, pp. 945–948, Pergamon, Oxford, U. K.

Tsyganenko, N. A. (2002a), A model of the magnetosphere with a dawn-dusk asymmetry 1. Mathematical structure, *J. Geophys. Res.*, *107*(A8), SMP 12-1–SMP 12-15, doi:10.1029/2001JA000219.

Tsyganenko, N. A. (2002b), A model of the near magnetosphere with a dawn-dusk asymmetry 2. Parameterization and fitting to observations, *J. Geophys. Res.*, *107*(A8), SMP 10-1–SMP 10-17, doi:10.1029/2001JA000220.

Tsyganenko, N. A. (2014), Data-based modeling of the geomagnetosphere with an IMF-dependent magnetopause, *J. Geophys. Res. Space Physics*, *119*, 335–354, doi:10.1002/2013JA019346.

Tsyganenko, N. A., and M. I. Sitnov (2005), Modeling the dynamics of the inner magnetosphere during strong geomagnetic storms, *J. Geophys. Res.*, *110*, A03208, doi:10.1029/2004JA010798.

Tsyganenko, N. A., and M. I. Sitnov (2007), Magnetospheric configurations from a high-resolution data-based magnetic field model, *J. Geophys. Res.*, *112*, A06225, doi:10.1029/2007JA012260.

Turner, N. E., D. N. Baker, T. I. Pulkkinen, and R. L. McPherron (2000), Evaluation of the tail current contribution to Dst, *J. Geophys. Res.*, *105*(A3), 5431–5439, doi:10.1029/1999JA000248.

Turner, N. E., W. D. Cramer, S. K. Earles, and B. A. Emery (2009), Geoefficiency and energy partitioning in CIR-driven and CME-driven storms, *J. Atmos. Sol. Terr. Phys.*, *71*, 1023–1031, doi:10.1016/j.jastp.2009.02.005.

Weygand, J. M., and R. L. McPherron (2006), Dependence of ring current asymmetry on storm phase, *J. Geophys. Res.*, *111*, A11221, doi:10.1029/2006JA011808.